NJC

ROYAL SOCIETY OF CHEMISTRY

PAPER

View Article Online
View Journal | View Issue

Cite this: *New J. Chem.*, 2025, 49, 10632

Inorganic–organic hybrid copper phosphate nanoflower coated with an upper rim tetra-imidazolyl-phenanthroline derivatized calix[4]arene: synthesis, characterization and its application as a peroxidase mimic catalyst†

Subrata Kumar Dinda,[a] Sivaiah Areti [b] and Chebrolu Pulla Rao ‡*[c]

An upper rim tetra-imidazolyl-phenanthroline derivatized calix[4]arene conjugate (**L**) was synthesized and characterized using different analytical, spectral, microscopic and diffraction techniques. The incubation of **L** with $CuSO_4{\cdot}5H_2O$ in PBS buffer (20 mM) for 1 h resulted in the formation of a nanoflower material. The **L**-coated copper phosphate nanoflowers (**L**@CuPNFs) were characterized through Fourier-transform infrared spectroscopy, X-ray photoelectron spectroscopy, powder X-ray diffraction, and microscopy techniques. The peroxidase mimetic activity of **L**@CuPNFs was assessed, and the results were compared with those of unmodified CuPNFs as a control. The peroxidase activity was demonstrated using three different substrates, *viz.*, tetramethylbenzidine (TMB), *ortho*-phenylenediamine (OPD) and guaiacol. The progress of the oxidation reaction of the model substrates in the presence of **L**@CuPNFs and H_2O_2 was demonstrated through absorption spectra measured as a function of time. The changes could be qualitatively gauged from the observed visual colour variation. The oxidized species were identified by measuring the ESI-MS spectrum of the reaction mixture. The rate of oxidation of these substrates in the presence of H_2O_2 was higher when **L**@CuPNFs were used as a catalyst, and this was much greater than the reaction rate observed with the unmodified CuPNF, which was not coated with **L**. All these results confirmed that the coating of **L** enhanced the peroxidase mimetic activity of the nanoflowers.

Received 13th February 2025,
Accepted 19th May 2025

DOI: 10.1039/d5nj00629e

rsc.li/njc

Introduction

Inorganic–organic hybrid nanoflower-like materials have gained significant attention owing to their unique structural properties and are involved in mimicking enzyme activity, such as that of peroxidases.[1–4] Upon immobilization of organic ligands and biomolecules on inorganic substrates, chemical and structural changes are induced in the corresponding nanomaterials to acquire newer properties. These functionalized nanoflower materials have shown significant advantages, such as enhanced operational stability, a high surface-to-volume ratio and improved biocatalytic performance.[5–7] Thus, nanoflower materials have been used for various applications, such as biosensing, targeted drug delivery, antibacterial treatment and enzyme-mimicking activity.[8–12] Therefore, developing nano-enzymes based on functionalized nanoflower materials has been a significant area of research.[13–15] Among nanoflower materials, copper phosphate $\{Cu_3(PO_4)_2\}$-based materials showed better enzyme mimicking activity in PBS buffer upon the incorporation of macromolecules.[16–18]

Macromolecules, such as proteins and polymers, have been used as stabilizing agents for the growth of nanomaterials, such as ZnO, CuO and $Cu_3(PO_4)_2$.[19–23] With careful optimization of the concentration of metal ions and stabilizing agents, nanomaterials with a specific size and shape and enhanced activity can be generated. When a similar strategy was adopted in the case of $Cu_3(PO_4)_2$, it resulted in the formation of nanoflowers with the use of organic molecules. Calixarenes have been extensively used as building blocks for the selective recognition of cations,[24,25] anions[26–28] and neutral molecules.[29–31] The upper rim and lower rim of calix[4]arene can be modified to serve various applications

[a] *Post Graduate Teacher (Chemistry), District CM School of Excellence Nadia Hindu School, Lohardaga, Jharkhand–835302, India*
[b] *Department of Chemistry, Sardar Vallabhbhai National Institute of Technology, Surat - Surat-Dumas Road, Surat-395007, India. E-mail: areti@chem.svnit.ac.in*
[c] *Department of Chemistry, School of Engineering and Applied Sciences, SRM University AP, Neerukonda (P.O.), Guntur (dist), Andhra Pradesh – 522240, India. E-mail: cprao@iittp.ac.in*

† Electronic supplementary information (ESI) available: Synthesis, ^{1}H NMR, ^{13}C NMR, ESI-MS characterization as well as fluorescence and absorption spectral data. See DOI: https://doi.org/10.1039/d5nj00629e

‡ Formerly at IIT Bombay followed by IIT Tirupati

in the area of host–guest interaction,[32] drug delivery[33,34] and catalysis.[35,36]

In this study, the upper rim of calix[4]arene is modified with four imidazolyl-phenanthroline moieties to decorate the macrocyclic platform and form multiple metal binding sites that would effectively coordinate Cu^{2+}. This work primarily focuses on the synthesis and characterization of conjugate **L** and a nanoflower material that is coated with the conjugate (**L**@CuPNF) and the application of the resultant inorganic–organic nanohybrid material as a peroxidase mimetic catalyst.

Experimental section

Materials and methods

All the reagents and chemicals were purchased from Sigma Aldrich Chemical Co., USA, and SRL, India, and were used without further purification. HPLC grade solvents were used for the spectral studies. ^{1}H and ^{13}C NMR spectra were recorded in $CDCl_3$ and DMSO-d_6 using a Bruker (400 or 500 MHz) NMR spectrometer. A Bruker spectrometer was used for the ESI-MS and HRMS spectra. Absorption spectra were measured using a Shimadzu UV2101PC spectrophotometer with a quartz cuvette cell. Freshly prepared stock solutions of **L**, **L**@CuPNF and CuNPF solution (1 mg ml^{-1} in all the cases) were prepared in PBS buffer (10 mM, pH 5.0) to perform the UV-vis studies. SEM images were taken using FE-SEM (Jeol Scanning Microscope JSM-6700F), and TEM micrographs were taken with the JEOL 2100F FEG-TEM instrument. The XPS spectra were measured using an AXIS Supra X-ray photoelectron spectrometer, Kratos Analytical, UK (225 W, pass energy 160 eV, and take off angle of 90°).

Synthesis and characterization of L

A mixture of $\mathbf{P_3}$ (0.536 g, 1.0 mmol, Schemes 1), 1,10-phenanthroline 5,6-dione (4.204 g, 20.0 mmol) and NH_4OAc (38.541 g, 500.0 mmol) was dissolved in glacial acetic acid (40 mL). The solution was refluxed for 48 h. The progress of the reaction was monitored by checking the TLC. The reaction mixture was allowed to cool to room temperature and was then poured into Milli-Q water (100 mL) to obtain the crude product as a precipitate. The precipitate was filtered and washed with Milli-Q water three times until the filtrate became neutral (*i.e.*, pH 7.0) and finally with CH_3OH two times and dried under vacuum to obtain a pure greenish-brown product of **L**. Yield 58% (0.75 g). ^{1}H-NMR (400 MHz, DMSO-d_6) δ (ppm): 13.44 (s, 4H), 9.26–8.92 (s, 16H), 8.05 (s, 8H), 7.24 (s, 8H), 4.61 (s, 4H), 3.66 (s, 4H); ^{13}C NMR (125 MHz, DMSO-d_6) δ (ppm): 157.09, 151.86, 151.64, 147.25, 142.882, 130.73, 130.55, 129.65, 126.90, 123.02, 120.12, 32.99; ESI-MS: *m*/*z* calculated for $C_{80}H_{48}N_{16}O_8$ is 1297.37, corresponding to $[M]^+$, and the observed *m*/*z* at 1297.34, corresponding to $[M]^+$. All the relevant spectra are presented in the ESI† (Fig. S3a–c).

Synthesis of L@CuPNF

The stock solutions of the conjugate (**L**) (1 mM) and that of the $CuSO_4{\cdot}5H_2O$ (100 mM) were prepared in DMSO and Milli-Q water, respectively. The Cu^{2+} solution was mixed with PBS buffer (20 mM) so that the concentration of Cu^{2+} was 5 mM, and the same concentration of Cu^{2+} was maintained in each sample. The solution of **L** was then added in different concentrations in the range of 0–100 μM to the Cu^{2+} ions dissolved in PBS solutions. The total volume of each sample was 1 mL. Upon the addition of **L**, the samples were kept undisturbed for 1 h. The precipitate was then washed twice with Milli-Q water and then dried under a vacuum.

Characterization of L@CuNFs

The nanoflowers of copper phosphate were characterized using microscopy techniques, such as transmission electron microscopy (TEM), by drop casting the solution on a copper grid and scanning electron microscopy (SEM) by drop-casting on an aluminum foil. The Fourier transform infrared (FTIR) spectra of the samples and the controls were measured as KBr pellets. Powder X-ray diffraction (PXRD) and X-ray photoelectron spectra (XPS) of samples drop-casted on the aluminum foil of the **L**@CuPNF and CuPNF were carried out.

Peroxidase mimetic activity of L@CuPNFs

The stock solutions of **L**@CuPNF (1 mg mL^{-1}) and CuPNF (1 mg mL^{-1}) were prepared in PBS buffer (10 mM, pH 5.0). A stock solution of H_2O_2 (100 mM) was prepared in Milli-Q water. The stock solutions of substrates, *viz.*, TMB (10 mM), OPD (10 mM) and guaiacol (1000 mM), were prepared in PBS buffer (10 mM, pH 5.0). The cuvette concentrations of **L**@CuPNF (0.1 mg mL^{-1}) and CuPNF (0.1 mg mL^{-1}) were fixed in each experiment. The cuvette concentrations of TMB (0.2 mM), OPD (0.2 mM) and guaiacol (40 mM) were used for their respective oxidation reactions. The cuvette concentrations of H_2O_2 were

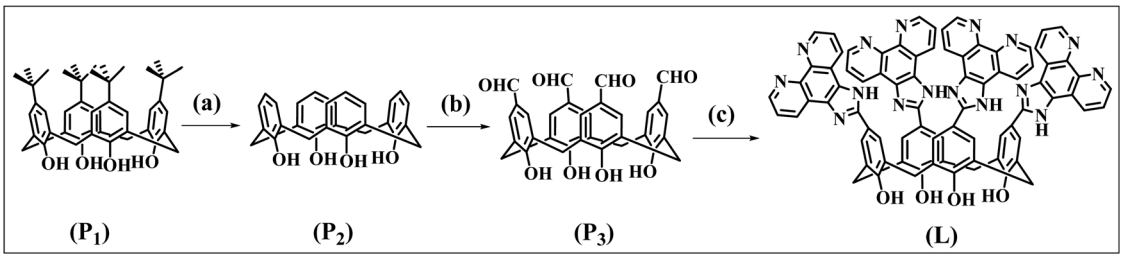

Scheme 1 Synthesis of **L**: (a) $AlCl_3$, phenol, toluene, RT, and 24 h; (b) hexamethylenetetramine (HMTA), trifluoroacetic acid (TFA), reflux, and 24 h; (c) 1,10-phenanthroline-5,6-dione, NH_4OAc, glacial AcOH, reflux, and 48 h.

2 mM for the oxidation of TMB and OPD and 20 mM for the oxidation of guaiacol.

Results and discussions

Tetra-imidazolyl-phenanthroline derivatized calix[4]arene, L

The **L** is synthesized *via* three steps, starting from *p-tert*-butyl calix[4]arene ($\mathbf{P_1}$), followed by dealkylation to yield $\mathbf{P_2}$, and $\mathbf{P_2}$ was converted to tetraformyl derivative, $\mathbf{P_3}$, which was finally condensed with 1,10-phenanthroline-5,6-dione to result in the desired compound (**L**), as shown in Scheme 1. The **L** and its precursors $\mathbf{P_2}$ and $\mathbf{P_3}$ were characterized by applying various spectroscopic techniques, including FT-IR, ^{1}H and ^{13}C-NMR, and ESI-MS. The corresponding data for $\mathbf{P_2}$, $\mathbf{P_3}$ and **L** are presented in the ESI† (Fig. S1–S3).

Synthesis and characterization of L@CuPNFs

The copper phosphate nanoflowers (CuPNFs) were synthesized at varying concentrations of **L** (0–100 μM), maintaining a fixed $CuSO_4{\cdot}5H_2O$ concentration (5 mM), and the product (L@CuPNFs) formed in each case was characterized by SEM, TEM, XPS, FTIR and PXRD. The corresponding results are presented in this section.

SEM characterization. The SEM micrographs of the product nanoflowers, **L@CuPNFs**, are depicted in Fig. 1a–d. It is found that the CuPNFs, without the presence of **L**, form flower-like morphology with a petal density of 240–280 petals per flower and that the size of the nanoflower is in the range of 16–19 μm. However, in the presence of 50 μM of **L**, the size of the nanoflowers is reduced to 8–12 μm, and the petal density also decreases to a large extent. When the ligand concentration increases to 100 μM, the petal density and the size of the nanoflowers are further reduced (Fig. 1e–h). All these data show that the presence of conjugate **L** affects the growth of the nanoflowers, making them smaller in size with a lower density of petals, which indicates a quick glueing action of **L** to the copper phosphate scaffold owing to the presence of four imidazolyl-phenanthroline moieties at the wider upper rim of the calix[4]arene, thereby providing a greater accessible reactive surface area for the reactants.

The growth of the nanoflowers with time evolution can be clearly observed, as shown in Fig. 2. The nanoflower formation was completed within 30 minutes of incubation, and all these nanoflowers were formed with the proper shape and size; no further change in the morphology of the nanoflowers was observed even after the incubation duration increased to 3 h.

TEM characterization. These **L**@CuPNFs were also characterized by TEM, and the flower-like morphology was also evident from TEM (Fig. 3a). The Cu^{2+} ions were embedded in the petals of these nanoflowers, as depicted in Fig. 3b. These CuPNFs are crystalline, as observed from the diffraction data, and the same can be observed in Fig. 3c. The coating of CuPNFs by **L** is confirmed by the presence of the corresponding elements noticed from the image mapping, and the corresponding images are illustrated in Fig. 3d–i.

XPS characterization. The hybrid supramolecular nanoflowers, **L**@CuPNFs, were further characterized by XPS (Fig. 4a–e). In **L**@CuPNFs, the binding energies of 2p electrons of Cu were altered significantly from those of uncoated nanoflowers alone, *viz.*, CuPNF. The peaks corresponding to Cu $2p_{3/2}$, Cu $2p_{1/2}$ and the Cu^{2+} satellite peaks were shifted towards lower energy by 0.99, 0.42 and 1.11 eV, respectively, ranging from CuPNFs to **L**@CuPNFs. Similarly, the binding energies of P 2p and O 1s of **L**@CuPNFs shift significantly when the molecules participate in the formation of NFs compared to those of unmodified CuPNF only. The peaks corresponding to P $2p_{3/2}$ and P $2p_{1/2}$ were shifted to the lower energy by 2.12 and 1.11 eV, respectively, in the case of **L**@CuPNFs when compared to

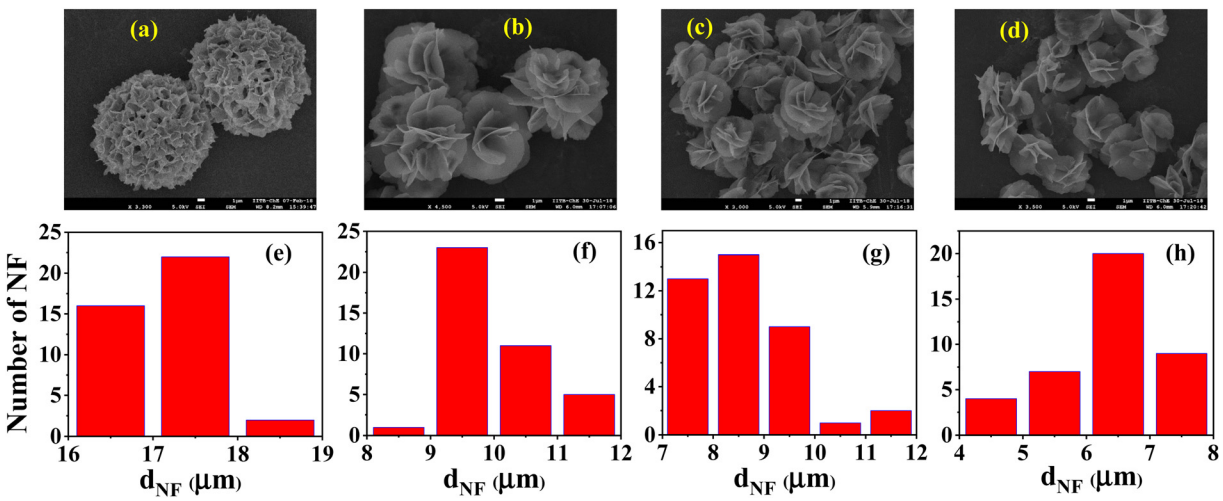

Fig. 1 SEM micrographs of (a) $Cu_3(PO_4)_2$ and **L**@CuPNFs with **L** concentrations of (b) 50 μM, (c) 75 μM and (d) 100 μM. (e)–(h): Size distribution of nanoflowers observed in (a), (b), (c) and (d). Scale bar (1 μm) is the same for all the micrographs. In the preparation of the nanoflowers, the concentrations of $CuSO_4$ and $5H_2O$ (5 mM) as well as the incubation period (1 h) were kept constant, and PBS buffer (20 mM, pH 7.4) was used in all the samples with different concentrations of **L**.

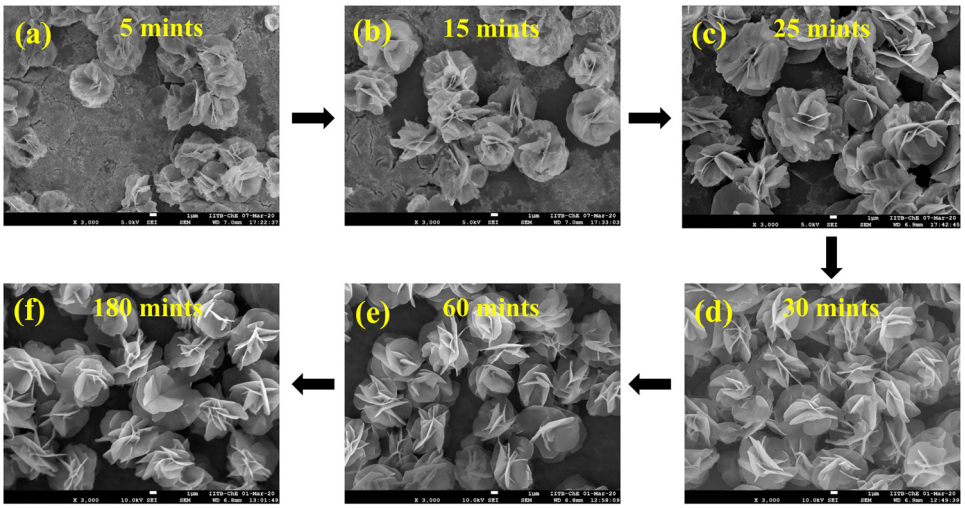

Fig. 2 (a)–(f) SEM micrographs of **L**@CuPNFs, depicting the growth of the nanoflowers at different times (5–180 minutes). The concentrations of **L** (75 μM) and $CuSO_4$, $5H_2O$ (5 mM) in PBS (20 mM, pH 7.4) were constant in all the samples. Scale bar is the same (*i.e.*, 1 μm) for each image.

CuPNFs. Similarly, the peaks for O 1s shifted to a lower energy by 1.05 and 1.07 eV, respectively. These spectral changes (Fig. 4f) clearly support the binding of **L** to the copper phosphate in the nanoflowers.

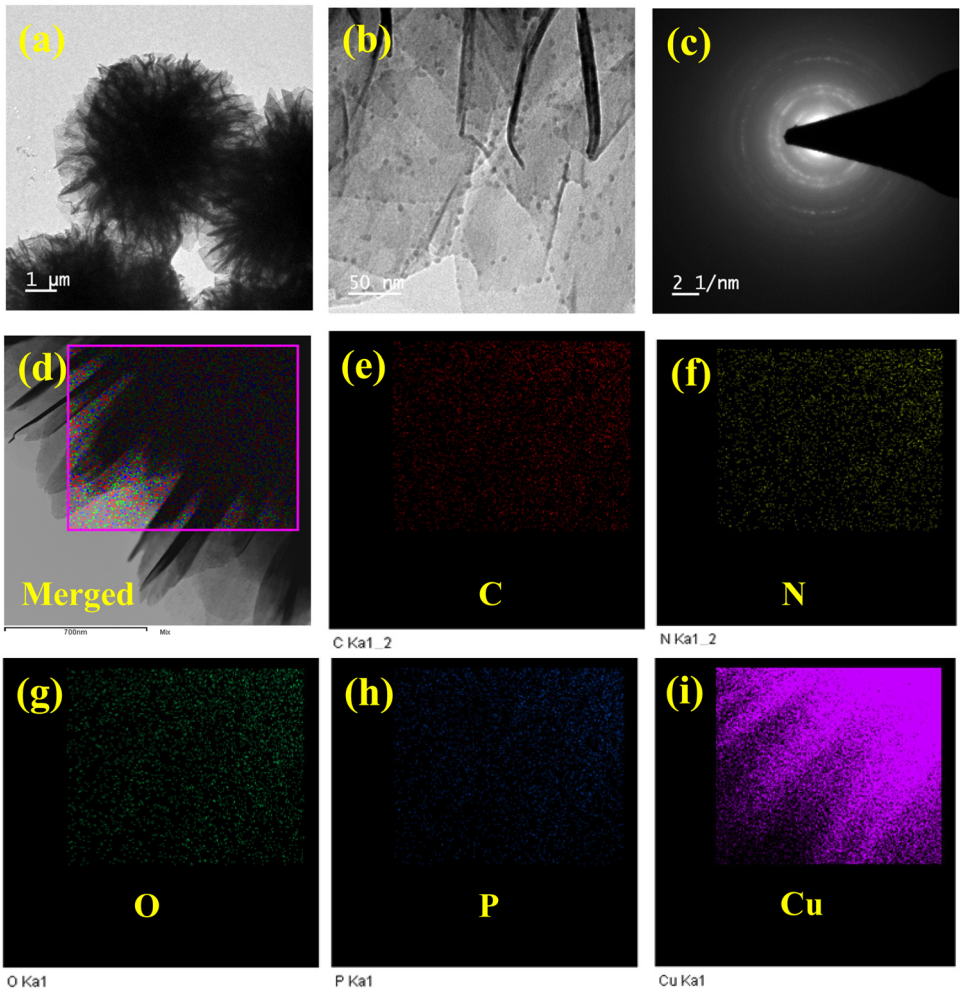

Fig. 3 TEM micrographs of **L**@CuPNFs at a scale bar of (a) 1 μm and (b) 50 nm. (c) Diffraction patterns of **L**@CuPNFs. (d) Merged image of the mapping of **L**@CuPNFs. Images of elements: (e) C; (f) N; (g) O; (h) P; (i) Cu.

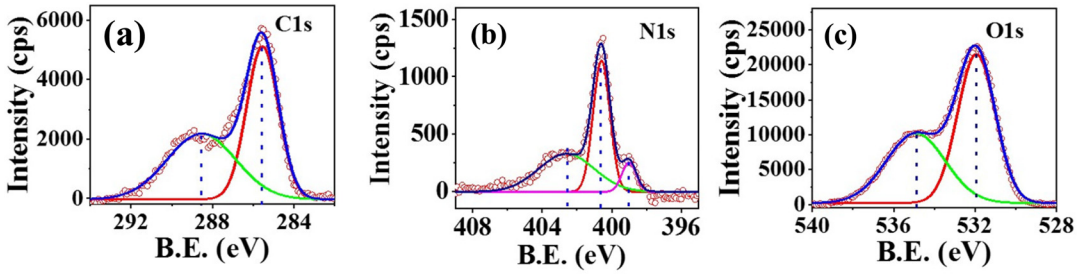

(f)

Elements	B.E (eV) L_5@CuPNF	B.E (eV) CuPNF
C	285.54, 288.54	
N	399.00, 400.59, 402.60	
O	531.93, 534.91	532.14, 535.98
P	133.83, 137.52	130.30, 135.95, 138.63
Cu	939.28, 946.46, 959.38, 967.00	940.27, 947.57, 959.80, 967.60

Fig. 4 XPS of **L**@CuPNFs: (a) C 1s, (b) N 1s, (c) O 1s, (d) P 2p and (e) Cu 2p. (f) Table comprising XPS binding energies (B. E.) for different elements of **L**@CuPNF and CuPNF samples.

FTIR characterization. **L**@CuPNFs were further characterized by FTIR, and the spectra were compared with those of **L** and CuPNF as controls (Fig. 5a). The FTIR spectrum of **L** shows bands at 1608, 1440, 1067, 807 and 740 cm^{-1} and that of CuPNFs at 1628, 1140, 1047, 987, 626 and 560 cm^{-1}. The FTIR spectrum of **L**@CuPNFs shows the presence of both the characteristic IR bands of CuPNF and **L** with considerable shifts, suggesting that **L** is anchored onto the copper phosphate in the nanoflowers.

Powder X-ray diffraction. Powder X-ray diffraction was carried out to confirm the crystalline nature of the CuPNFs. It is observed that the diffraction pattern is almost unaltered in the hybrid nanomaterial, **L**@CuPNFs, as shown in Fig. 5b. However, the lines were broadened. The peak positions were further confirmed by comparing them with the JCPDS data. Thus, the FT-IR and PXRD data together provided evidence for the presence of both **L** and hydrated copper phosphate, $Cu_3(PO_4)_2.3H_2O$, in the nanoflower products.

Peroxidase mimetic activity of L@CuPNFs

To demonstrate peroxidase mimetic activity, the researchers generally used the following three substrates: 3,3,5,5-tetramethylbenzidine (TMB), *ortho*-phenylenediamine (OPD) and guaiacol. Therefore, in the present study, we take these three as the substrate models to demonstrate the peroxidase mimetic activity of our synthetic nano-hybrid catalyst, **L**@CuPNF, based on absorption spectral studies, as reported in this section. To compare the peroxidase mimetic activity of our synthetic nano-hybrid catalyst, **L**@CuPNF, we performed similar absorption spectral measurements with the control molecule, *i.e.*, just **L** alone with all the three substrates, and the spectra are reported in the ESI† (Fig. S4). In the presence of conjugate **L**, even for a longer time of up to 120 min, the absorption spectra showed no significant change, and no oxidation product was formed by conjugate **L** in the presence of H_2O_2, suggesting that **L** alone did not show any peroxidase activity. The results are the same for all the three substrates. As demonstrated in this study, **L**-coated nanoflower, *i.e.*, **L**@CuPNFs, exhibited enhanced peroxidase-like activity with all these three substrates.

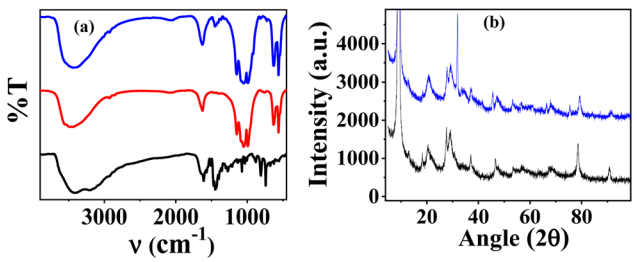

Fig. 5 (a) FT-IR spectra of **L** (black line), CuPNFs (red line) and **L**@CuPNFs (blue line). (b) PXRD of CuPNFs (black line) and **L**@CuPNFs (blue line).

3,3,5,5-Tetramethylbenzidine (TMB) as a substrate

According to the reported literature,[37–40] copper phosphate nanoflowers exhibit peroxidase-like activity, where TMB is used as a model substrate, and a similar methodology is applied in the present case. When TMB is used as the substrate, it is converted to blue coloured oxidized-TMB product upon reaction with H_2O_2 in the presence of **L**@CuPNFs as a catalyst, as can be observed from the colour of the solutions of the vials and the corresponding photograph of the vials illustrated in Scheme 2(a). The ESI-MS showed a peak at m/z = 241.20 supporting the formation of the oxidized TMB product (Fig. S5, ESI†). The product formation is monitored spectrophotometrically by following the absorption peak of the product at 650 nm. Only in the presence of 0.1 mg ml^{-1} of catalyst,

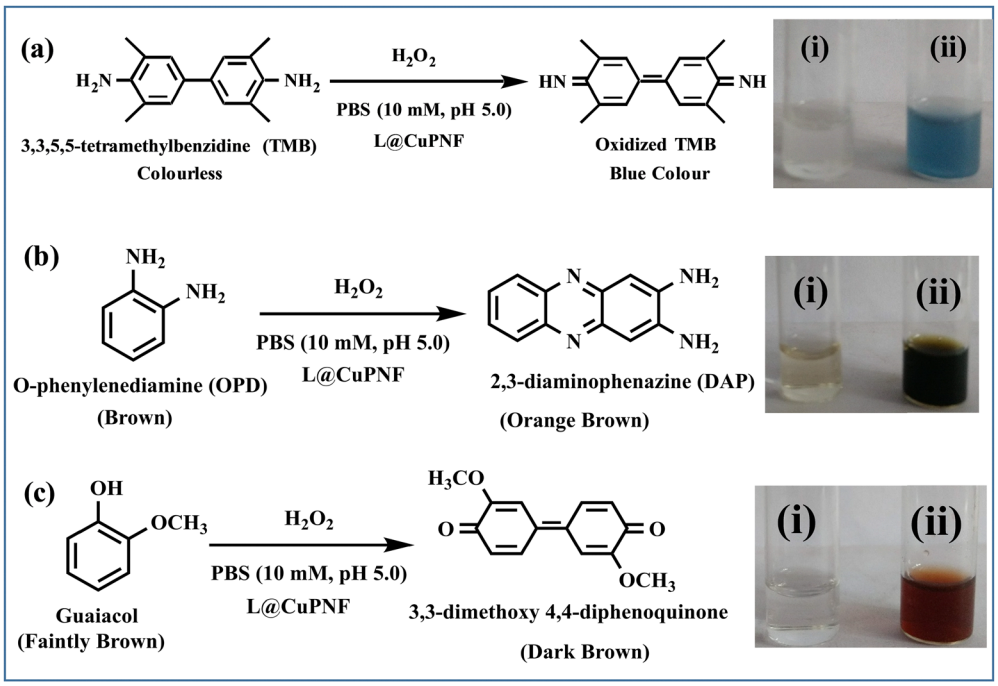

Scheme 2 Oxidation reaction of (a) TMB, (b) OPD and (c) guaiacol in the presence of H_2O_2 and the **L**@CuPNF catalyst. In the photograph of the vials, (i) and (ii) correspond to the reactant and products in PBS (10 mM, pH 5.0), respectively.

i.e., **L**@CuPNFs, the oxidation reaction is completed within 10 min while giving a new band at 650 nm, which increases with time and the absorbance remains the same thereafter, and this can be observed from Fig. 6a. In a similar experiment carried out with unmodified CuPNFs (without being coated with **L**), the absorbance saturates only beyond 15 min at a slower rate. The expedited rate of oxidation of TMB in the presence of H_2O_2 catalysed by **L**@CuPNFs compared to unmodified CuPNF (Fig. 6b) can be understood from the plots illustrated in Fig. 6c. If the time taken to achieve half the absorbance value is used for comparison, the rate of the reaction shows an increase of 200% with **L**-coated CuNFs compared to the use of unmodified CuNFs. The data confirm that the **L**@CuPNFs are more efficient catalysts than unmodified CuPNFs owing to the anchoring of **L**.

Ortho-phenylenediamine (OPD) as substrate

Similar studies were carried out using OPD as the model substrate. The oxidation reaction of OPD was carried out in the presence of H_2O_2 using **L**@CuPNF, and additional experiments were carried out using appropriate controls for data comparison. The formation of the oxidized product of OPD, *viz.*, 2,3-diaminophenazine, is shown in Scheme 2b. The product formation is supported by the ESI-MS spectrum, which exhibits a peak at m/z = 211.13 that corresponds to this product (Fig. S6, ESI†). The progress of the reaction is monitored by recording the absorption spectra, wherein the oxidized product exhibits a band at 440 nm. The absorbance increases with respect to time, and the absorbance value is unaltered beyond 25–30 min. This can be observed in Fig. 6d–f. The colour change from light brown to orange-brown was observed during the reaction, and the same can be noticed from the photographs of the vials shown in Scheme 2b. A comparison of the absorbance plots reveals that the rate of conversion of *ortho*-phenylenediamine to 2,3-diamino phenazine is expedited by 150% in the case of **L**@CuPNF when compared to the use of unmodified CuPNF without **L** coating as a catalyst.

Guaiacol as a substrate

Guaiacol is also used as another model substrate for studying peroxidase-like activity, and a similar protocol is also adapted in the present case. The oxidation reaction is shown in Scheme 2c, and product formation is observed through the band at 475 nm in the absorption spectra. All these are further accompanied by a visual colour change from light brown to dark brown, as can be noticed from the photographs of the vials given in Scheme 2c. The reaction mixture obtained upon completion of the kinetics study was used for ESI-MS measurement. The spectrum showed a peak corresponding to the oxidized product of guaiacol at m/z = 269.10, and this was assigned to $[M + Na]^+$. (Fig. S7, ESI†). The absorbance of the product band at 475 nm increases with respect to time; further, the absorbance is unaltered beyond 50–60 min. Comparison of the absorption spectral data reveals that the **L**-coated CuPNF (*i.e.*, **L**@CuPNF) takes the reaction through an expedited rate of oxidation by 130% higher when compared to the use of unmodified CuPNF, and the corresponding spectra and the absorption plots are depicted in Fig. 6g–i. Thus, with all the three substrates studied, the oxidation reaction is expedited in the presence of the CuPNFs coated with **L** compared to the unmodified CuPNFs, thus strongly suggesting that **L** is involved in enhancing the oxidation reaction.

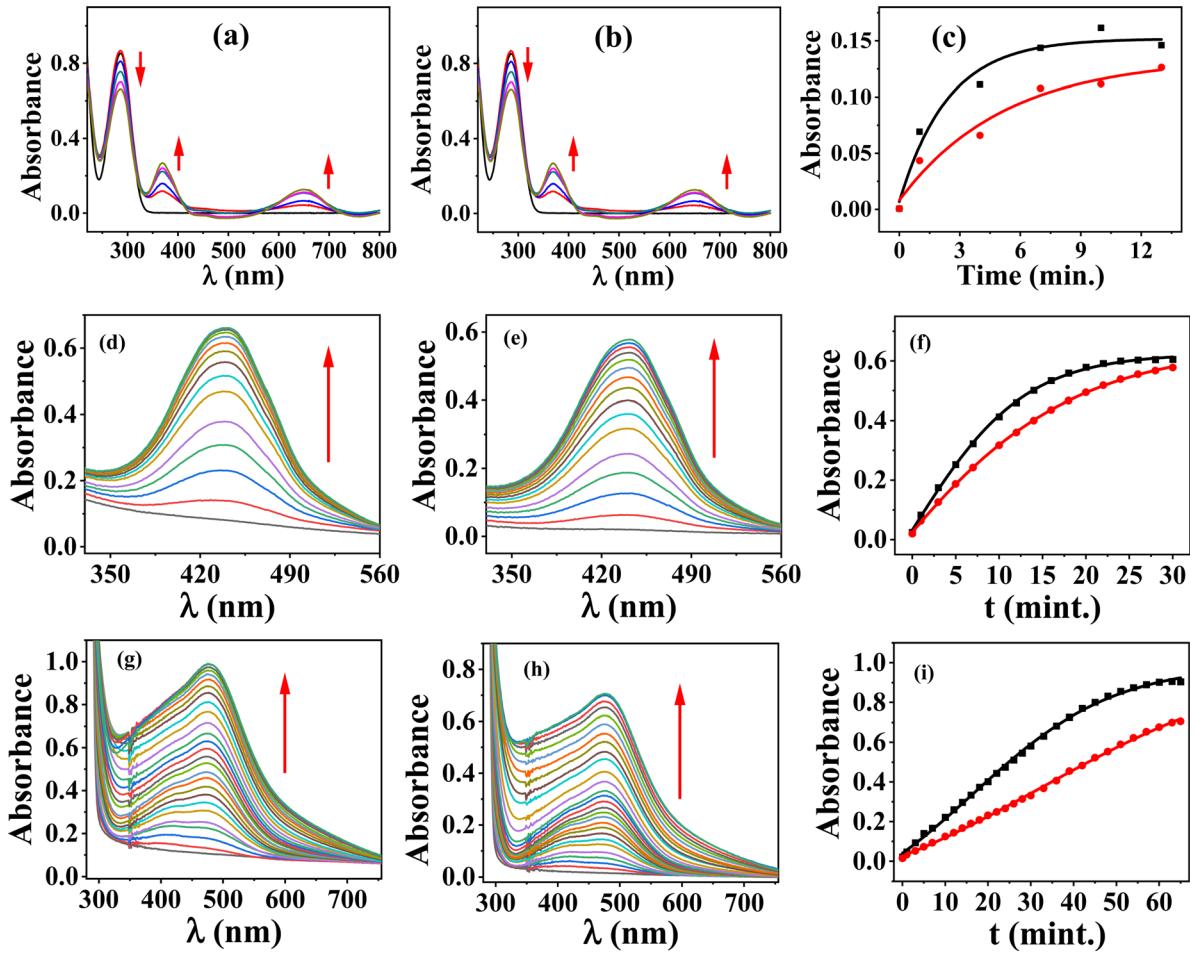

Fig. 6 Peroxidase mimetic activity: UV-visible spectra of TMB in the presence of H_2O_2 and (a) **L**@CuPNFs or (b) unmodified CuPNFs at different times; (c) plot of absorbance at 650 nm *versus* time, wherein black and red traces correspond to **L**@CuPNF- and CuPNF-catalyzed reactions, respectively. UV-visible spectra of OPD in the presence of H_2O_2 and (d) **L**@CuPNFs or (e) unmodified CuPNFs at different times. (f) Plot of absorbance at 440 nm *versus* time, wherein the black and red traces correspond to **L**@CuPNF- and CuPNF-catalyzed reactions, respectively. UV-visible spectra of guaiacol in the presence of H_2O_2 and (g) **L**@CuPNFs or (h) CuPNFs at different times. (i) Plot of absorbance at 475 nm *versus* time, wherein the black and red traces correspond to **L**@CuPNF- and CuPNF-catalyzed reactions, respectively.

Conclusions and comparisons

The ligand, **L**, possessing four imidazolyl-phenanthroline moieties on the upper rim of calix[4]arene, was synthesized and characterized by ^{1}H and ^{13}C NMR and ESI-MS. The ligand is designed to possess nitrogen groups at the upper rim to express its binding capacity to various transition metal ions, including Cu^{2+}. The design of the molecular system helps in the optimization of the growth of CuPNFs through their 'N' centers, while the calix[4]arene moiety helps to stabilize the structure of CuNFs, thereby increasing the rate of peroxidase activity. Nanoflower formation and growth were monitored and characterized using microscopy techniques. At a concentration of 50 μM of **L**, the growth of the nanoflowers was regulated to shrink their size to half (8–12 μm) with a concomitant decrease in the density of petals. All these are attributable to a rapid glueing action of **L** to the copper phosphate scaffold, which is in turn formed through imidazole-fused phenonthroline moieties at the upper rim. This results in a greater accessible reactive surface area, thereby expediting the reaction in the case of **L**-coated CuPNFs compared to unmodified CuPNFs. This is well demonstrated in the present study through its peroxidase mimetic activity.

These **L**@CuPNFs were utilized for peroxidase mimetic activity, as demonstrated using TMB, OPD and guaiacol as model substrates. The peroxidase mimetic activity exhibited a 2-fold increase in the rate of oxidation of TMB in the presence of H_2O_2 catalyzed by **L**@CuPNFs compared to unmodified CuPNF, as demonstrated based on absorption spectral study. The oxidation reaction was further demonstrated using other model substrates, such as OPD and guaiacol, in the presence of **L**@CuPNF and H_2O_2 through similar absorption spectral measurements. The product formation was further confirmed through ESI mass spectrometry. All these findings suggest that the calix[4]arene conjugate, **L**, possessing four imidazolyl–phenanthroline moieties used in the present study, stabilizes the complex formed with copper centers present in the nanoflowers. The **L** alone does not show any peroxidase mimetic activity even for longer durations of the reaction times with all the three substrates. To eliminate the

influence of Cu^{2+} precursors, similar studies carried out using $CuSO_4$ and $Cu(acac)_2$ showed no significant contribution to peroxidase activity. The corresponding data are available in the ESI† (Fig. S9). Therefore, the enhanced peroxidase mimetic activity was attributed to the presence of the coated calixarene conjugates, *viz.*, **L** on CuPNFs (*i.e.*, **L**@CuPNFs). There are no systems reported for the peroxidase mimetic activity of **L**@CuPNF, where **L** = conjugate of calixarene. However, we found in the literature a few systems of **L**@CuPNFs that show peroxidase mimetic activity, and in those cases the L is not a calix-derivative, and the corresponding data are presented in the ESI† as Fig. S8 with Table S1. It is believed that the development of inorganic–organic hybrid materials, such as **L**@CuPNFs, is important to generate catalyst materials in peroxidase-mimicking applications, as demonstrated beyond doubt in this study.

Conflicts of interest

There are no conflicts of interest to declare.

Acknowledgements

CPR acknowledges the Department of Science and Technology for J. C. Bose National Fellowship, IIT Tirupati for MHRD Professorship and SRM University AP for the current position as Senior Professor. CPR expresses his gratitude to IIT Bombay for fostering his academic and research activities for over three decades (1988–2019) and for Institute Chair Professorship during 2011–2019. AS gratefully acknowledges the Science and Engineering Research Board (SERB) for a Start-up Research Grant (SRG) SRG/2023/1723. SKD acknowledges CSIR for the Senior Research Fellowship {09/087(0796)/2014-EMR-I}, which was awarded at IIT Bombay during his PhD tenure.

References

1 C. A. S. Ballesteros, L. A. Mercante, A. D. Alvarenga, M. H. M. Facure, R. Schneider and D. S. Correa, Recent trends in nanozymes design: from materials and structures to environmental applications, *Mater. Chem. Front.*, 2021, **5**, 7419–7451.

2 J. Wu, X. Wang, Q. Wang, Z. Lou, S. Li, Y. Zhu, L. Qin and H. Wei, Nanomaterials with enzyme-like characteristics (nanozymes): next-generation artificial enzymes (II), *Chem. Soc. Rev.*, 2019, **48**, 1004–1076.

3 J. Chen, Z. Guo, Y. Xin, Z. Gu, L. Zhang and X. Guo, Organic-inorganic hybrid nanoflowers: A comprehensive review of current trends, advances, and future perspectives, *Coord. Chem. Rev.*, 2023, **489**, 215191.

4 I. G. Subramani, V. Perumal, S. C. B. Gopinath, K. S. Fhan and N. M. Mohamed, Organic-Inorganic Hybrid Nanoflower Production and Analytical Utilization: Fundamental to Cutting Edge Technologies, *Crit. Rev. Anal. Chem.*, 2021, 1–23.

5 N. Narkhede, B. Uttam and C. P. Rao, Silica–Calix Hybrid Composite of Allyl Calix[4]arene Covalently Linked to MCM-41 Nanoparticles for Sustained Release of Doxorubicin into Cancer Cells, *ACS Omega*, 2019, **4**, 4908–4917.

6 A. G. Thawari and C. P. Rao, Peroxidase-like Catalytic Activity of Copper-Mediated Protein− Inorganic Hybrid Nanoflowers and Nanofibers of β-Lactoglobulin and α-Lactalbumin: Synthesis, Spectral Characterization, Microscopic Features, and Catalytic Activity, *ACS Appl. Mater. Interfaces*, 2016, **8**, 10392–10402.

7 J. Cui and S. Jia, Organic–inorganic hybrid nanoflowers: A novel host platform for immobilizing biomolecules, *Coord. Chem. Rev.*, 2017, **352**, 249–263.

8 R. Zhang, B. Jiang, K. Fan, L. Gao and X. Yan, Designing nanozymes for in vivo applications, *Nat. Rev. Bioeng.*, 2024, **2**, 849–868.

9 J. Zhang, W. Qian, C. Kong and F. Wei, Increasing para-Xylene Selectivity in Making Aromatics from Methanol with a Surface-Modified Zn/P/ZSM-5 Catalyst, *ACS Catal.*, 2015, **5**, 2982–2988.

10 Y. Liu, X. Jia and Z. He, Organic-inorganic nanoflowers: from design strategy to biomedical applications, *Nanoscale*, 2019, **11**, 17179–17194.

11 A. K. Singh, K. Bijalwan, N. Kaushal, A. Kumari, A. Saha and A. Indra, Oxidase-like Nanozyme Activity of Manganese Metal–Organic Framework Nanosheets for Colorimetric and Fluorescence Sensing of l-Cysteine, *ACS Appl. Nano Mater.*, 2023, **6**, 8036–8045.

12 X. Liang, Y. Liu, K. Wen, W. Jiang and Q. Li, Immobilized enzymes in inorganic hybrid nanoflowers for biocatalytic and biosensing applications, *J. Mater. Chem. B*, 2021, **9**, 7597.

13 C. Shang, Q. Wang, H. Tan, S. Lu, S. Wang, Q. Zhang, L. Gu, J. Li, E. Wang and S. Guo, Defective PtRuTe As Nanozyme with Selectively Enhanced Peroxidase-like Activity, *JACS Au*, 2022, **2**, 2453–2459.

14 S. Ray, R. Biswas, R. Banerjee and P. Biswas, A gold nanoparticle-intercalated mesoporous silica-based nanozyme for the selective colorimetric detection of dopamine, *Nanoscale Adv.*, 2020, **2**, 734–745.

15 C. Cong, Y. C. He, S. X. Zhao, X. W. Zhang, L. Li, D. S. Wang, L. X. Liu and D. W. Gao, Diagnostic and therapeutic nanoenzymes for enhanced chemotherapy and photodynamic therapy, *J. Mater. Chem. B*, 2021, **9**, 3925–3934.

16 Y. Ni, Z. Sun, Z. Zeng, F. Liu and J. Qin, Hydrothermal fabrication of hierarchical CuO nanoflowers for dual-function amperometric sensing of hydrogen peroxide and glucose, *New J. Chem.*, 2019, **43**, 18629–18636.

17 M. Li, J. Chen, W. Wu, Y. Fang and S. Dong, Oxidase-like MOF-818 Nanozyme with High Specificity for Catalysis of Catechol Oxidation, *J. Am. Chem. Soc.*, 2020, **142**, 15569–15574.

18 Z. Zhang, H. Che, Y. Wang, J. Gao, X. She, J. Sun, Z. Zhong and F. Su, Flower-like CuO microspheres with enhanced catalytic performance for dimethyldichlorosilane synthesis, *RSC Adv.*, 2012, **2**, 2254–2256.

19 Y. Xu, J. Jin, X. Li, Y. Han, H. Meng, T. Wang and X. Zhang, Simple synthesis of ZnO nanoflowers and its photocatalytic

performances toward the photodegradation of metamitron, *Mater. Res. Bull.*, 2016, **76**, 235–239.
20 R. M. Tripathi, A. S. Bhadwal, R. K. Gupta, P. Singh, A. Shrivastav and B. R. Shrivastav, ZnO nanoflowers: novel biogenic synthesis and enhanced photocatalytic activity, *J. Photochem. Photobiol., B*, 2014, **141**, 288–295.
21 N. M. Rana, S. Ahmedi, R. Mehandi, M. Dhama and N. Manzoor, and Rahisuddin. Transition metal complexes of benzimidazole-based ligands: Synthesis, characterization, biological, and catecholase activities, *Inorg. Chim. Acta*, 2025, **574**, 122392.
22 D. Feng, Z. Y. Gu, J. R. Li, H. L. Jiang, Z. Wei and H. C. Zhou, Zirconium-Metalloporphyrin PCN-222: Mesoporous Metal–Organic Frameworks with Ultrahigh Stability as Biomimetic Catalysts, *Angew. Chem., Int. Ed.*, 2012, **51**, 10307–10310.
23 Y. Huang, X. Ran, Y. Lin, J. Ren and X. Qu, Self-assembly of an organic–inorganic hybrid nanoflower as an efficient biomimetic catalyst for self-activated tandem reactions, *Chem. Commun.*, 2015, **51**, 4386–4389.
24 A. Llamosí, M. P. Szymański and A. Szumna, Molecular vessels from preorganised natural building blocks, *Chem. Soc. Rev.*, 2024, **53**, 4434–4462.
25 R. K. Pathak, J. Dessingou, V. K. Hinge, A. G. Thawari, S. K. Basu and C. P. Rao, Quinoline Driven Fluorescence Turn On 1,3-Bis-calix[4]arene Conjugate-Based Receptor to Discriminate Fe3+ from Fe2+, *Anal. Chem.*, 2013, **85**, 3707.
26 H. Ren, H. Wang, W. Wen, S. Li, N. Li, F. Huo and C. Yin, A summary of calixarene-based fluorescent sensors developed during the past five years, *Chem. Commun.*, 2023, **59**, 13790–13799.
27 B. Uttam, R. Kandi, M. A. Hussain and C. P. Rao, A fluorescent lower rim 1, 3-di-benzooxadiazole conjugate of calix[4]arene in selective sensing of fluoride in solution and in biological cells using confocal microscopy, *J. Org. Chem.*, 2018, **83**, 11850.
28 A. Nehra, A. Malik, P. R. Sharma, S. Bandaru and R. K. Sharma, Rapid naked eye sensing of fluoride by calix[4]arene upper rim tetra functionalized pentafluorophenyl hydrazone, *New J. Chem.*, 2023, **47**, 13080–13083.
29 Q. Sun, Y. Lu, L. Liu, K. Liu, R. Miao and Y. Fang, Experimental Studies on A New Fluorescent Ensemble of Calix[4]pyrrole and Its Sensing Performance in the Film State, *ACS Appl. Mater. Interfaces*, 2016, **8**, 29128–29135.
30 J. C. Barnes, M. Juricek, N. L. Strutt, M. Frasconi, S. Sampath, M. A. Giesener, P. L. McGrier, C. J. Bruns, C. L. Stern., A. A. Sarjeant and J. F. Stoddart, A Polycyclic Aromatic Hydrocarbon Scavenger, *J. Am. Chem. Soc.*, 2013, **135**, 183.
31 H. Zhu, L. Shangguan, B. Shi, G. Yu and F. Huang, Recent progress in macrocyclic amphiphiles and macrocyclic host-based supra-amphiphiles, *Mater. Chem. Front.*, 2018, **2**, 2152–2174.
32 R. Kumar, A. Sharma, H. Singh, P. Suating, H. S. Kim, K. Sunwoo, I. Shim, B. C. Gibb and J. S. Kim, Revisiting Fluorescent Calixarenes: From Molecular Sensors to Smart Materials, *Chem. Rev.*, 2019, **119**, 9657–9721.
33 S. B. Nimse and T. Kim, Biological applications of functionalized calixarenes, *Chem. Soc. Rev.*, 2013, **42**, 366–386.
34 R. Jean-Noël, C. Benoit, B. Olivia, O. Diana and R. Olivia, Biomimetic cavity-based metal complexes, *Chem. Soc. Rev.*, 2015, **44**, 467–489.
35 F. J. Ruiz-Mendoza, C. D. Emmanuel, A. H. Alejandro and M. E. Daniel, Synthesis and catalytic applications of NHC–metal complexes supported on p-tert-butylcalix[4]arene frameworks, *New J. Chem.*, 2024, **48**, 14021–14028.
36 G. J. Cao, X. Jiang, H. Zhang, T. R. Croley and J. J. Yin, Mimicking horseradish peroxidase and oxidase using ruthenium nanomaterials, *RSC Adv.*, 2017, **7**, 52210–52217.
37 M. L. Li, L. Liu, Y. Shi, Y. F. Yang, H. Z. Zheng and Y. J. Long, Dichlorofluorescein as a peroxidase mimic and its application to glucose detection, *New J. Chem.*, 2017, **41**, 7578–7582.
38 Z. Lin, Y. Xiao, Y. Yin, W. Hu, W. Liu and H. Yang, Facile Synthesis of Enzyme-Inorganic Hybrid Nanoflowers and Its Application as a Colorimetric Platform for Visual Detection of Hydrogen Peroxide and Phenol, *ACS Appl. Mater. Interfaces*, 2014, **613**, 10775–10782.
39 B. Somturk, M. Hancer, I. Ocsoy and N. Özdemir, Synthesis of copper ion incorporated horseradish peroxidase-based hybrid nanoflowers for enhanced catalytic activity and stability, *Dalton Trans.*, 2015, **44**, 13845–13852.
40 J. N. Shang, X. Li, Y. H. Ren, H. X. Ding, J. P. Cao, R. He, B. Yue and H. Y. He, A one-dimensional chain of manganese(II) bridgedperoxomolybdate isolated from an aqueous Mn–polymolybdate–H_2O_2 system, *Dalton Trans.*, 2023, **52**, 10058–10063.

